# The Deformation of Spherical Vesicles with Permeable, Constant-Area Membranes: Application to the Red Blood Cell

K. H. Parker and C. P. Winlove

Physiological Flow Studies Group, Department of Biological and Medical Systems, Imperial College of Science, Technology and Medicine, London SW7 2BY, U.K.

ABSTRACT   The deformation of an initially spherical vesicle of radius $a$ with a permeable membrane under extensive forces applied at its poles is calculated as a function of the in-plane shear modulus, $H$, and the out-of-plane bending modulus, $B$, using an axisymmetric theory that is valid for large deformations. Suitably nondimensionalized, the results depend upon a single nondimensional parameter, $C \equiv a^2 H/B$. For small deformations, the calculated force–polar strain curves are linear and, under these conditions, the slope of the curve determines only $C$, not the values of $H$ and $B$ separately. Independent determination of $H$ and $B$ from experimental measurements require deformations that are large enough to produce nonlinear behavior. Simple approximations for large and small $C$ are given, which are applied to experimental measurements on red blood cell ghosts that have been made permeable by treatment with saponin.

## INTRODUCTION

The mechanical properties of plasma membranes have been shown in recent years to play an important part in physiology and cell biology. An archetypal system for study is the red blood cell membrane, the elastic character of which determines many of the flow properties of blood and enables the red blood cells to transverse the capillaries. Although the red cell is, in some sense, unique, in that it contains no cytoplasmic cytoskeleton or organelles, the complexes of the proteins that make up its associated membrane skeletal network and give it its elastic properties occur in plasma membranes of other cell types. An example is the sarcolemma, in which dystrophin is thought to act as an elastic component, resembling the erythroid elastomeric protein, spectrin. Thus, in cells of dystrophic muscle, in which the dystrophin is missing or defective, the elasticity of the membrane is much reduced (Pasternak et al., 1995). It has been argued (Dai and Sheetz, 1998) that membrane tension controls such processes as cell shape and motility, as well as endo- and exocytosis, and, in several cell types, tensile forces applied to the membrane induce extensive metabolic changes. To understand the mechanism of these various effects, the elastic characteristics of plasma membranes need to be defined in explicit and not merely empirical terms. Techniques, such as optical tweezers and atomic force microscopy, are now being widely explored to augment more conventional approaches to the study of membrane mechanics, notably micropipette aspiration. The most tractable system for study by these means is a closed spherical membrane, such as can be generated by lysis of a red cell. We develop here a theory to allow evaluation of elastic properties from force–extension relations measured on a system of this type. The accompanying paper (Sleep et al., 1999) illustrates the application of the theory.

The classic theoretical analysis of micropipette aspiration experiments by Evans and his colleagues argued that the bending modulus was negligible compared to the shear modulus (Evans and Skalak, 1980) and this approximation has been incorporated in many more recent theoretical analyses (Hansen et al., 1997; Boey et al., 1998). However, the theoretical treatments of other membrane phenomena, such as the formation of tethers (Waugh et al., 1992; Bozic et al., 1997), spicules (Iglic, 1997) and undulatory excitations (Zeman et al., 1990) take the opposite view and emphasize the importance of bending stiffness of the membrane. In interpreting data such as those from the laser tweezers experiments it is not clear which approximation is most appropriate.

We have chosen to analyze the problem by inclusion of both shear and bending moduli using the approach of Pamplona and Calladine (1993), which was developed to analyze pressure-induced deformation of lipid vesicles. This approach was considered appropriate primarily because it is a large-deformation theory, formulated in terms of unambiguously defined membrane properties.

An essential assumption of the theory is that the membrane has a locally constant area under deformation and so its mechanical behavior can be described by two material constants, an out-of-plane bending modulus, $B$, which describes the resistance to bending, and an in-plane shear modulus, $H$, which describes the resistance to changes of shape in the plane of the membrane. Pamplona and Calladine (1993) relate the bending modulus in their lipid bilayers to a change of area modulus in the individual layers, but, because of the presence of the cytoskeleton in the red blood cell, we take the bending modulus as a primitive property of the cell membrane, dependent upon both the mechanics of the lipid bilayer and the cytoskeleton. Indeed, one of the principal goals of our investigation is to interpret the effect of changes in the composition and organization of the

cytoskeleton on the mechanical response of the cell. Therefore, throughout the paper, we shall use "membrane" to refer to the lipid bilayer, its integral proteins, and associated membrane skeleton.

## DEVELOPMENT OF THE GOVERNING EQUATIONS

We shall assume that the cell is spherical and isotropic in its resting configuration and that extensive loads are applied at diametrically opposed points, which we will refer to as the poles. We assume that the deformation under this load is axisymmetrical. With this assumption, it is natural to adopt the meridional and circumferential directions as the principal directions, designated by the subscripts $s$ and $\theta$, respectively. The radius of the undeformed cell, $a$, will be taken as the reference length and used to nondimensionalize all lengths in the problem. The meridian of the cell is shown in Fig. 1 in its original, spherical configuration and in a deformed configuration. The undeformed cell is described in polar, cylindrical coordinates $(r, z)$ with $z$ directed between the poles. The arc length along the meridian, $s$, will be taken as the independent variable in the final equations. In the undeformed configuration, $s$ is also the angle from the pole measured from the center of the sphere. The coordinates for the deformed sphere are $(R, Z)$, the arc length along the meridian is $S$, and the angle from the pole measured from the local center of curvature is $\phi$.
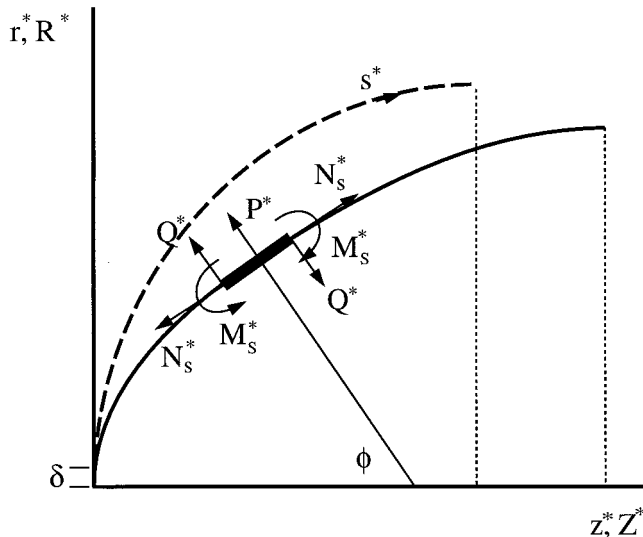


FIGURE 1   A sketch of the undeformed (*dashed*) and deformed (*solid*) meridional geometry of the axisymmetric cells. $r^*$ and $z^*$ are the radial and axial coordinates, and $s^*$ is the arc-length coordinate in the undeformed, spherical cell. $R^*$, $Z^*$, and $S^*$ are the equivalent coordinates in the deformed cell. $P^*$ is the pressure acting normal to the membrane element, which is at angle $\phi$ from the polar axis. $N_s^*$ is the meridional stress resultant, $Q^*$ is the out-of-plane shear stress resultant, and $M_s^*$ is the meridional bending moment per unit length of membrane. For the sake of clarity, the circumferential stress resultant, $N_\theta^*$ and bending moment, $M_\theta^*$ are not shown. It is assumed that the distending force is applied at the poles in the form of a constant pressure $P_0$ applied over the small radius $\delta$.

## Geometry

The relationship between the undeformed and deformed geometry of the cell can be seen from Fig. 1. All dimensional variables are denoted with an asterisk.

$$r^* = \sin s^* \tag{1}$$

$$z^* = 1 - \cos s^* \tag{2}$$

$$\frac{\mathrm{d}R^*}{\mathrm{d}S^*} = \cos \phi \tag{3}$$

$$\frac{\mathrm{d}Z^*}{\mathrm{d}S^*} = \sin \phi \tag{4}$$

The curvatures in the meridian and circumferential directions, $\kappa_s^*$ and $\kappa_\theta^*$, are

$$\kappa_s^* = \frac{\mathrm{d}\phi}{\mathrm{d}S^*}, \tag{5}$$

$$\kappa_\theta^* = \frac{\sin \phi}{R^*}. \tag{6}$$

## Equations of equilibrium

The equations describing the equilibrium configuration of the cell membrane are derived in Pamplona and Calladine (1993), and the reader is referred to their paper for the details of the derivation. It is assumed that the membrane is locally constant in area and isotropic and that its elastic properties can be characterized by two moduli, the shear modulus $H$ ($N/m$), which describes the stiffness of the membrane to changes in shape in the plane of the membrane, and the bending modulus $B$ ($Nm$), which describes the resistance of the membrane to bending. The nondimensional ratio of these two moduli, $C \equiv a^2 H/B$, plays an important role in the analysis. The forces and torques acting on an element of the deformed membrane are indicated in Fig. 1. $P^*$ is the pressure ($N/m^2$), $N_s^*$ and $N_\theta^*$ are the meridional and circumferential stress resultants ($N/m$), $Q^*$ is the out-of-plane shear stress resultant ($N/m$), and $M_s^*$ and $M_\theta^*$ are the meridional and circumferential bending moment per unit length ($N$). For the sake of clarity, the circumferential stress and bending moment, $N_\theta^*$ and $M_\theta^*$, are omitted from Fig. 1.

We assume that the membrane stresses can be written as

$$N_s^* = T^* + \frac{H}{\lambda} \tag{7}$$

$$N_\theta^* = T^* + H\lambda, \tag{8}$$

where $\lambda = R^*/r^*$ is the local circumferential strain and, by the assumption that the membrane is locally of constant area, $1/\lambda$ is the local meridional strain. $T^*$ is the membrane stress resultant and is one of the dependent variables in the problem. These constitutive equations correspond to the assumption of linear elasticity of the membrane and will be

questionable for large deformations. In the limit of a locally constant area membrane, the bending moments in the meridional and circumferential directions are equal and depend upon the bending modulus, $B$, and the mean curvature $\kappa_s^* + \kappa_\theta^*$,

$$M_s^* = M_\theta^* = B(\kappa_s^* + \kappa_\theta^*). \tag{9}$$

In a departure from the formalism of Pamplona and Calladine (1993), we chose to nondimensionalize the equations using $a$ and $H$ instead of $a$ and $B$. Thus, $R = R^*/a$, $Z = Z^*/a$, $\kappa = a\kappa_s^*$, $P = aP^*/H$, $Q = Q^*/H$, and $T = T^*/H$. (The use of the same symbols for differently defined nondimensional variables could cause some confusion when referring to Pamplona and Calladine. The nondimensional equations in Pamplona and Calladine can be obtained from our equations by replacing our variables $P$, $Q$, and $T$ by $P/C$, $Q/C$, and $T/C$ to reflect the different scalings.) With this nondimensionalization, the equations describing the geometry and the mechanical equilibrium of the membrane are

$$R' = \lambda^{-1}\cos \phi \tag{10}$$

$$Z' = \lambda^{-1}\sin \phi \tag{11}$$

$$\phi' = \lambda^{-1}\kappa \tag{12}$$

$$\kappa' = \lambda^{-1}[-CQ + R^{-2}\sin \phi \cos \phi - \kappa R^{-1}\cos \phi] \tag{13}$$

$$Q' = \lambda^{-1}[P - (T + \lambda^{-1})\kappa \\ - (T + \lambda)R^{-1}\sin \phi - QR^{-1}\cos \phi] \tag{14}$$

$$T' = \lambda^{-1}[(\lambda - \lambda^{-1})R^{-1}\cos \phi + \kappa Q] \\ - R^{-1}\cos s + R^{-3}\cos \phi \sin^2 s \tag{15}$$

where the prime denotes differentiation with respect to $s$. Eqs. 10–12 simply relate the deformed membrane geometry to the initial spherical geometry. The circumferential strain is

$$\lambda \equiv \frac{R}{r} = \frac{R}{\sin s}. \tag{16}$$

By the assumption that the membrane is locally of constant area, the strain in the meridional direction satisfies

$$\frac{dS}{ds} = \frac{1}{\lambda}, \tag{17}$$

and this relationship is used to transform derivatives with respect to the deformed arc length, $S$, to derivatives with respect to $s$.

Eqs. 13–15 describe the equilibrium of forces in the direction normal to the membrane and tangential to the meridional direction and moments normal to the meridional direction in terms of the dependent variables: the curvature in the meridional direction, $\kappa$, the torque acting on a meridional element, $Q$, and the membrane stress resultant, $T$.

## Boundary conditions

To avoid the complications introduced by point loads, it is assumed that the force is applied to the cell membrane in the form of a uniform pressure, $P_0^*$, applied over a small region of radius $\delta^*$ at the poles, so that $F^* = \pi\delta^2 P_0^*$. Outside this small region, it is assumed that the transmural pressure is zero, reflecting the permeability of the cell membrane in the experimental tests. The boundary conditions follow most easily from an analysis of the symmetry at $s = 0$. $R$, $\phi$, and $Q$ are odd functions at the poles while all of the other variables are even, and thus $R(0) = \theta(0) = Q(0) = 0$. Also, from the definition of the coordinate system, $Z(0) = 0$. The final two boundary conditions occur on the equator, $s = \pi/2$, where, by symmetry, $\phi(\pi/2) = \pi/2$ and $Q(\pi/2) = 0$.

Applying the boundary conditions and a small $s$ expansion to all of the variables, we find the conditions at $s = \delta \equiv \delta^*/a$, the edge of the area over which the force is applied

$$R(\delta) = \delta \tag{18}$$

$$Z(\delta) = 0 \tag{19}$$

$$\phi(\delta) = \kappa_0\delta \tag{20}$$

$$\kappa(\delta) = \kappa_0 \tag{21}$$

$$Q(\delta) = Q_0'\delta \tag{22}$$

$$T(\delta) = (\tfrac{1}{2}P_0 - Q_0')\kappa_0^{-1} - 1 \tag{23}$$

where the final equation follows from the differential equation for $Q$ at the pole, Eq. 14.

## Limit behavior

### The $B \to 0$ limit

Most previous studies of red cell membrane mechanics have been based on analyses that assume that the bending modulus is so small that its effect can be neglected (Evans and Skalak, 1980). The most common experiments to which this analysis has been applied involves sucking a portion of the membrane into a micropipette and observing the amount of distortion as a function of the pressure. This experiment is very different mechanically from the experiments that we are trying to model, but, nevertheless, it is of interest to explore the behavior of our analysis in the limit $B \to 0$. Using a nondimensionalization based on $H$ rather than $B$ enables us to look more easily at this limit.

As $B \to 0$, $C \to \infty$, and we see from Eq. 13 that the continuity of $\kappa'$ requires that $Q = 0$. Because $Q(0) = 0$, this can be satisfied if $Q' = 0$ and Eq. 14 reduces to the ordinary equation,

$$0 = P - (T + \lambda^{-1})\kappa - (T + \lambda)R^{-1}\sin \phi, \quad \text{as} \quad C \to \infty. \tag{24}$$

This relationship is identical to that developed by previous workers when the bending modulus was neglected (Evans and Skalak, 1980, Eq. 3.7.2, p.66).

For a membrane loaded at its poles, in the limit $C \rightarrow \infty$, the assumption of constant area thus implies that there can be no deformation of the spherical membrane as $F$ increases. The membrane stress is given by Eq. 24, $P = 2(T + 1)$.

### The $H \rightarrow 0$ limit

The other limit of interest is the liquid membrane, which has a bending moment but negligible resistance to shape changes in the plane of the membrane. Unfortunately, the limit of $C \rightarrow 0$ is difficult to study with our choice of nondimensionalization, and so we report results for $C \rightarrow 0$ by reverting to the Pamplona and Calladine (1993) nondimensionalization. In this limit, we have been unable to find simplifications of the basic equations.

## Numerical methods

The problem can be solved by a shooting method. In addition to the boundary conditions, we assume a value of the curvature, $\kappa(0) \equiv \kappa_0$, and the initial gradient of the bending moment, $Q'(0) \equiv Q'_0$. The differential equations are solved by marching to $s = \pi/2$ and the values of $\phi(\pi/2)$ and $Q(\pi/2)$ are calculated. This process is continued iteratively until the boundary conditions at the equator are satisfied.

The system of equations is highly nonlinear, and some care must be taken in the selection of initial conditions if convergence is to be attained. For given initial conditions, the equations are integrated from $s = \delta$ to $\pi/2$ using an explicit one-step Runge–Kutta method (Matlab function ode23). We have defined an error function, $\chi^2 = (\phi(\pi/2) - \pi/2)^2 + Q(\pi/2)^2$, and used the simplex method to minimize $\chi^2$ below a chosen tolerance value (Jacoby et al., 1972). The tolerance value was taken as $10^{-6}$ for the calculations presented here, although the results were found to be insensitive to the choice of tolerance.

The value of $\delta$, the radius of the circle around the pole over which the extensive force is applied, was taken as $\delta = 0.01$ for the calculations presented here. The sensitivity of the results to the choice of $\delta$ was tested over a wide range of values, keeping $P_0 = F/\pi\delta_2$. The differences between the results for $\delta < 0.01$ were smaller than the chosen error tolerance.

## RESULTS

Figure 2 shows the shape of the cell calculated for $C = 0$, 1, 10, and 100 for a series of increasing extensive forces. As expected, the cell becomes increasingly prolate as the force increases. As $C$ increases, the curvature near the poles increases, and the deformed cell becomes more pointed at the same strain. For the largest strains for large $C$, the

meridional profiles develop a point of inflection. The stress–strain curves calculated for a range of values of $C$ are shown in Fig. 3, where $F$ is plotted against the polar strain, $\varepsilon_p \equiv Z(\pi/2) - 1$ (*solid lines*) and equatorial strain, $\varepsilon_e \equiv R(\pi/2) - 1$ (*dotted lines*). For $C < 50$, the curves are complete in the sense that strains above the maximum values shown are possible, but they occur at lower values of $F$. This bifurcation of solutions will be discussed further below. At larger $C$, the curves at larger values of $F$ become increasingly difficult to calculate because the equations become stiffer (in the terminology of numerical analysis) and the convergence of the shooting procedure is very sensitive to the accuracy of the initial guesses. We note that the nonlinear behavior of the force–strain curves are qualitatively different for large and small $C$. For large $C$, the cells become stiffer as they are extended. For small $C$, the cells become less stiff with extension.

Because of our choice of nondimensionalization, the results for $F^* = 0$ cannot be included in Fig. 3, and so, we also present the results of our calculations in terms of the rescaled force $CF$. Figure 4 shows $CF$ as a function of the polar strain, $\varepsilon_p$, for $C = 0$, and the other values of $C$ shown in Fig. 3. For the smaller values of $C$, we also found equilibrium configurations involving large deformations. As an example, Fig. 5 shows results calculated for $C = 0$ where a sequence of biconcave equilibrium configurations were found.

The nesting of the $F - \varepsilon$ curves for different values of $C$ suggested that, for small polar strains, the force is primarily dependent upon the bending stiffness, $B$, with the in-plane membrane stiffness, $H$, contributing relatively little to the polar stiffness of the cells. This, in turn, suggests that $F$ at a given polar strain will depend linearly upon $1/C$. Figure 6 shows $F$ for $\varepsilon_p = 0.1$ plotted against $1/C$ where, indeed, the relationship is remarkably linear for $C < 50$. From the slope and intercept of the linear portion of this curve, we conclude that

$$F \approx \left(\frac{16}{C} + 1.4\right)\varepsilon_p \tag{25}$$

for small strains and $C < 50$. In dimensional terms, this is equivalent to

$$F^* \approx \left(\frac{16B}{a} + 1.4aH\right)\varepsilon_p. \tag{26}$$

This indicates that, when $C < 50$, the in-plane shear stiffness has a simple additive effect on the force required to produce a given strain. This is largely because the local deformed shape is mainly a consequence of the bending stiffness, which makes the surface as rounded as possible. Note that the different dimensions of $B$ and $H$ mean that the cell radius has an inverse effect on the magnitude of the two terms.

For $C > 10$, we find that, by rescaling the force as $C^{1/3}F$ the calculated stress–strain curves reduce very nearly to a single curve as shown in Fig. 7. In dimensional terms, this
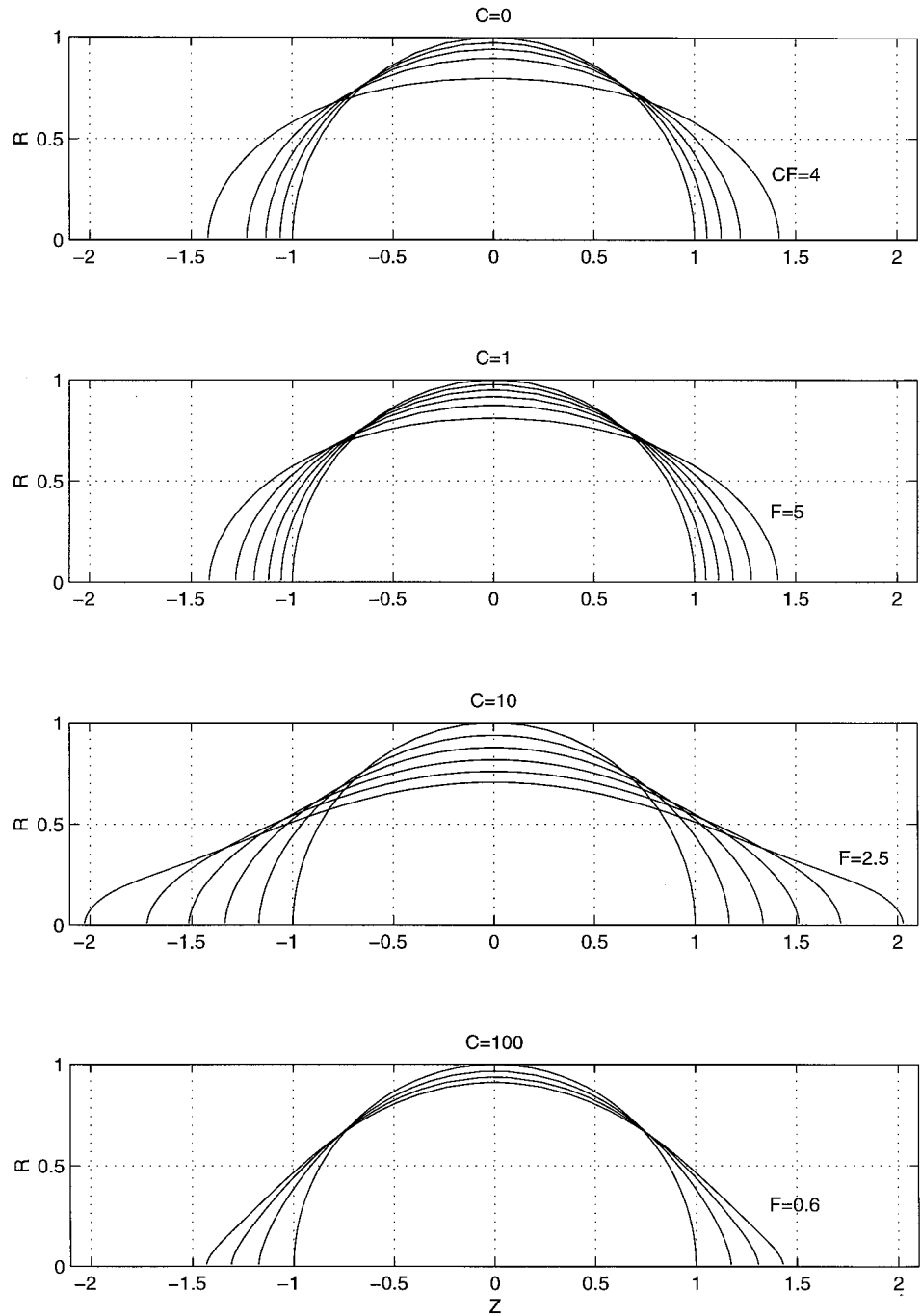
FIGURE 2 Calculated meridional profiles at different distending forces for different values of C. (*A*) $C = 0$, $CF = 0$, 1, 2, 3, and 4. (*B*) $C = 1$, $F = 0$, 1, 2, 3, 4, and 5. (*C*) $C = 10$, $F = 0$, 0.5, 1, 1.5, 2, and 2.5. (*D*) $C = 100$, $F = 0$, 0.2, 0.4, and 0.6.

scaling corresponds to

$$F_S \equiv C^{1/3}F = \frac{F^*}{(aBH^2)^{1/3}}. \qquad (27)$$

That is, there seems to be a natural, or characteristic, scale for the force, $(aBH^2)^{1/3}$, which governs the problem when $C > 10$. Although the relationship is only empirical, it is of some practical use, in that we observe from Fig. 7 that $F_S \approx 0.5$ for $\varepsilon_p = 0.1$, and this enables us to deduce a relationship between $H$ and $B$ from an experimental force–strain curve by measuring the force at 10% strain. In dimensional terms,

this is equivalent to

$$F^* \approx 5(aBH^2)^{1/3}\varepsilon_p. \qquad (28)$$

Unlike the case for small $C$, the polar stiffness of the cell depends upon a product of the two moduli when $C > 10$. We note, however, that, in both cases, the slope of the initial, linear portion of the force–polar strain curve determines only a relationship between $B$ and $H$ and does not allow us to determine either parameter uniquely. To determine either modulus uniquely, we require experimental
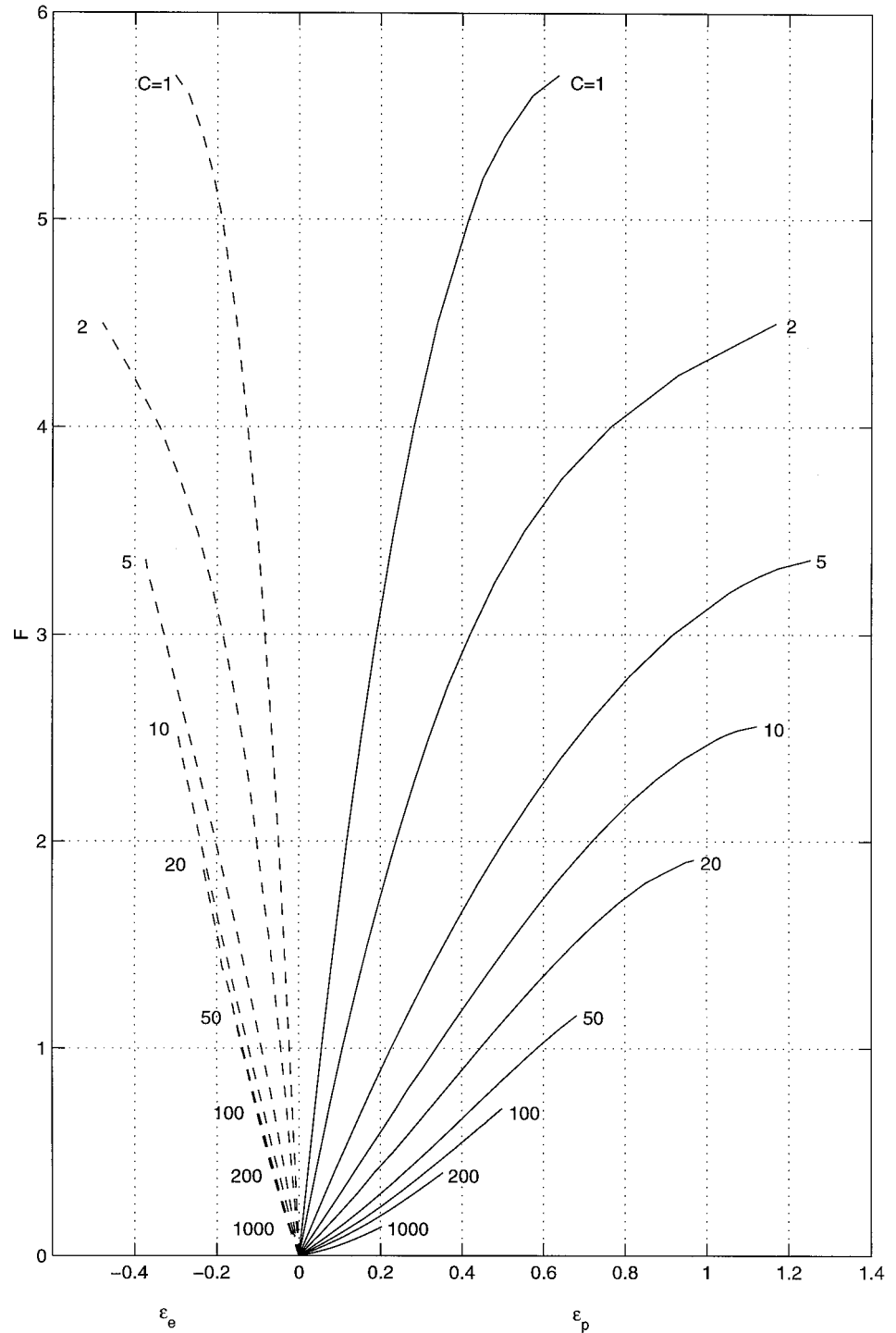
FIGURE 3 Calculated force–distension curves. $F$ is the nondimensional force, $\varepsilon_p$ is the polar strain (*solid lines*) and $\varepsilon_p$ is the equatorial strain (*dashed lines*). The values of $C$ are indicated next to each curve. For $C < 50$, the curves are complete in the sense that no solutions for higher $F$ could be found involving incremental changes in cell shape. For $C > 50$, the curves are terminated arbitrarily (see text).

measurements over a larger range of strains where the nonlinear behavior could be used to determine both moduli.

## DISCUSSION

The principal finding of this study is the intricate interaction of the shear modulus and the bending modulus in determining the deformation of a spherical cell. The dimensions of the two moduli are different, and so, their relative importance depends upon the cell radius. In nondimensional terms, the cell membrane mechanics are governed by the single parameter, $C = a^2 H / B$.

Although the theory allows for a pressure difference across the membrane, the results presented here are for the case of a permeable membrane, which, at equilibrium, cannot support a pressure difference. Because most previous

FIGURE 4 The rescaled force $CF$ as a function of polar strain, $\varepsilon_p$ for different values of $C$. Note that, with this scaling, it is possible to calculate a force–extension curve for $C = 0$.
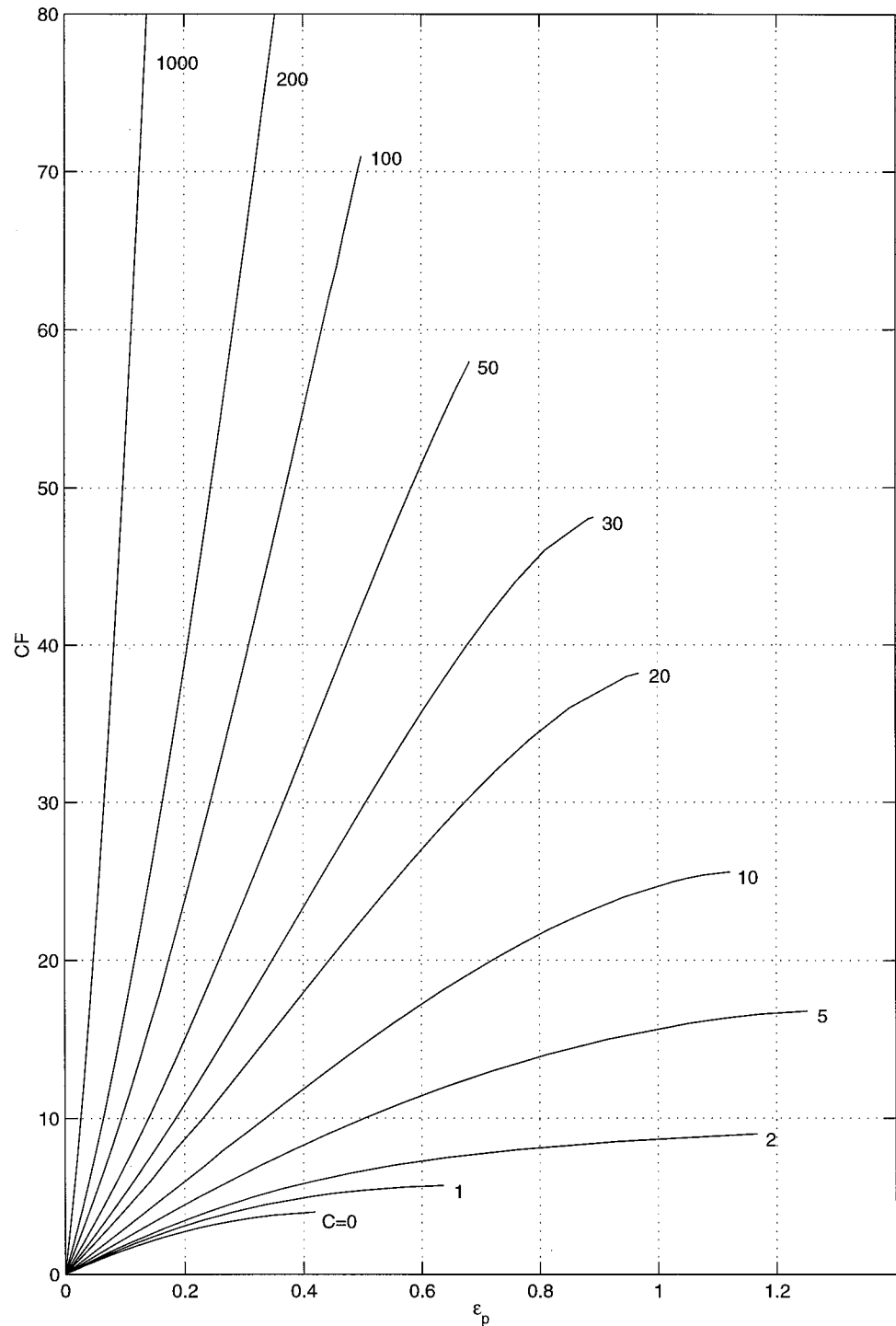
studies have considered the membranes to be impermeable, we have not been able to find other theoretical results for comparison. However, we expect that the mechanics of the permeable membrane will be more sensitive than the impermeable membrane to changes in the shear and bending moduli. The constant volume condition for the impermeable membrane is a very strong constraint, which could dominate the equilibrium cell configuration independently of the elastic moduli. The permeable membrane is free of the constant

volume constraint, and so we believe that the changes in configuration with load will be more sensitive to changes in the elastic moduli.

The basic equations presume axisymmetry but are valid for large deformations. However, the simple linear constitutive equations are less likely to be valid at large deformations, so the results presented here for the larger strains must be viewed with caution. It would be easy to incorporate more complex, nonlinear constitutive equations into the
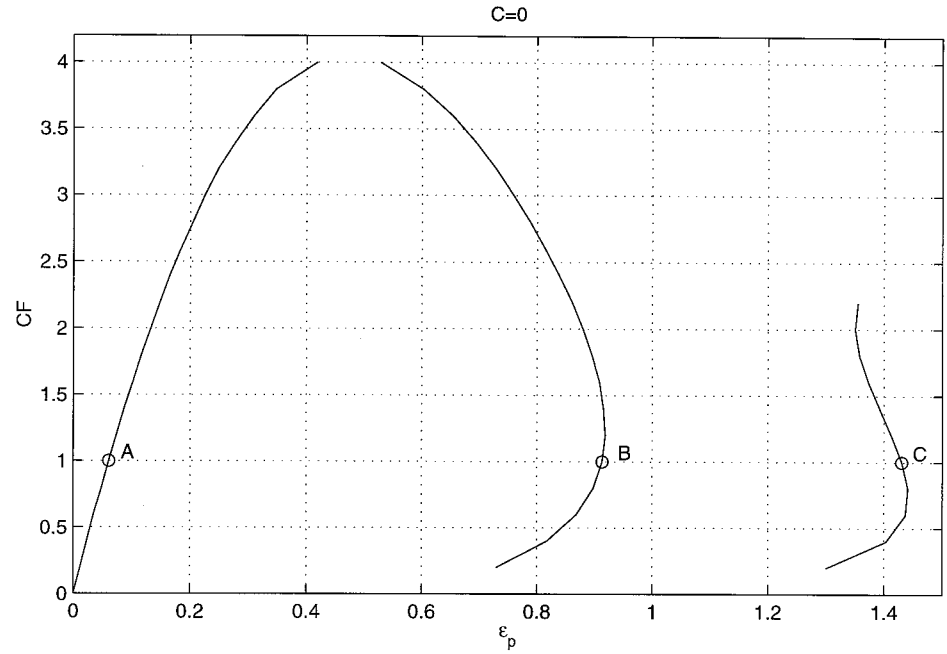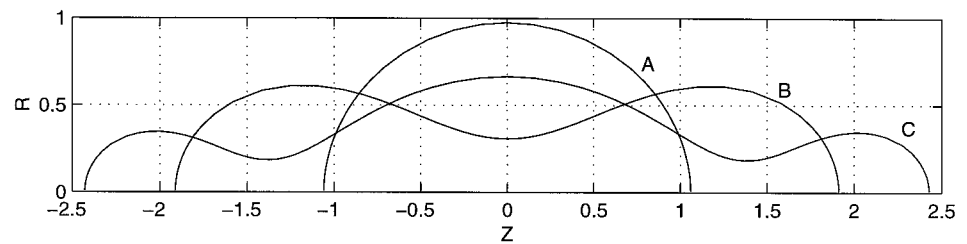
FIGURE 5 (*A*) The rescaled force *CF* as a function of polar strain, $\varepsilon_p$ for $C = 0$, showing three separate branches of solutions. The curve at low $\varepsilon_p$ corresponds to the curve shown in Fig. 4. The points labeled A, B, and C denote the conditions for which the profiles are shown. (*B*) The meridional cell profiles for the conditions A, B, and C indicated in (*A*).

formulation, but, at present, there is no evidence on what nonlinear elastic laws would be valid, so we have not pursued this possibility.

We have confidence in the theoretical results for the smaller strains. The numerical solutions are well behaved and insensitive to the choice of parameters such as the convergence criterion. The solution is also independent of the choice of the polar region over which the extending force was applied, the pressure varying with $\delta^2$ over a wide range of radii. For small strains, the solutions converged rapidly and were fairly independent of the initial guesses for $\kappa_0$ and $Q_0'$. In all cases, the convergence of the numerical scheme was checked using the convergence values as initial guesses. For larger strains, the equations became considerably more stiff and were very dependent upon good initial guesses for convergence. Nevertheless, once convergence was attained, the solutions were stable.

A significant result of the analysis is that it is impossible to determine both of the moduli *B* and *H* from the linear portion of an experimental force–polar strain measurement. Although the nondimensional equations are a function of the single parameter *C*, the use of one or other of the moduli in the nondimensionalization means that it is only possible to determine a relationship between the two moduli from the slope of the force–polar strain curve. The two approximations given by Eqs. 26 and 28 for small and large values of *C* should provide a useful way to determine the relationship between *B* and *H* practically. For small *C*, Eq. 26 indicates that the polar stiffness of the cell depends approximately linearly upon *B* with the in-plane membrane stiffness contributing in an additive fashion. The linearity of the relationship up to values of $C \approx 50$, seen in Fig. 6, is somewhat surprising but convenient, because it means that the ranges of validity of the two approximations overlap considerably.
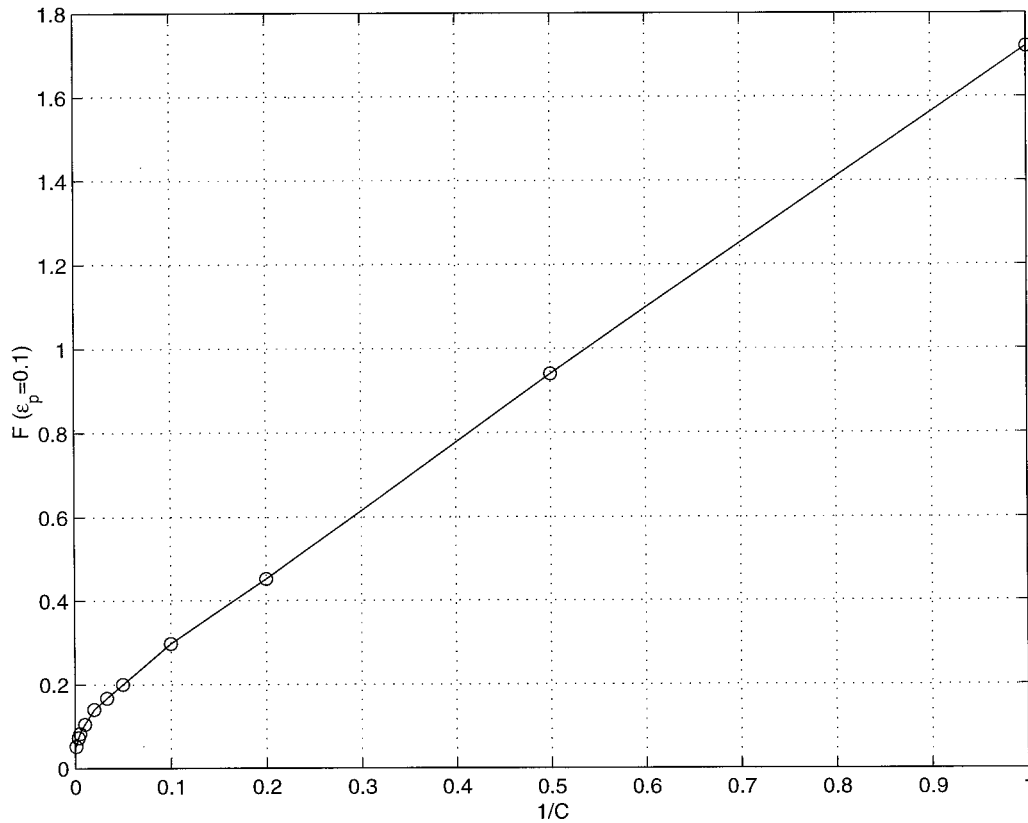
FIGURE 6   $F$ at $\varepsilon_p = 0.1$ plotted against $1/C$. The points indicate conditions for which data were calculated. The slope and intercept of the linear portion of this curve are indicated in Eq. 25.

For $C > 10$, the observation that the force–extension curves reduce nearly to a single curve when the force is scaled by the characteristic force $(aBH^2)^{1/3}$ leads to the approximation for large $C$ given by Eq. 28. We have not found an analytical reason for this scaling and emphasize that it is an approximate rather than exact result.

The large deformation solutions, seen, for example in Fig. 5, indicate the presence of bifurcations and multiple solutions of the equilibrium equations. We have not explored the higher-order branches of the solutions in any detail. For $C = 0$, there were at least 3 distinct branches corresponding to the configurations shown in the figure, and other string-of-pearls configurations may exist. The first bifurcation seems to appear where the slope of the force–polar strain curve goes to zero, although the difficulty of obtaining convergence in this region of the calculations makes it difficult to explore this question with our program.

For $C < 30$, the termination of the force–polar strain curves shown in Figs. 3 and 4 correspond to the highest forces for which an equilibrium solution could be found. We presume that there are branches similar to those seen for $C = 0$, although this was not explored. For $C > 50$ the end-points of the curves shown in Figs. 3 and 4 are arbitrary, and we expect that they will continue to higher forces. The $C = 50$ curve seems to be near to the boundary where the curvature changes from concave to the strain axis to

concave to the force axis. That is, for $C < 50$, the polar stiffness of the cell decreases as it is strained and for $C > 50$ it increases, at least as far as we were able to continue the calculations. This difference in the nonlinear behavior of the curves may provide a way of experimentally determining both $B$ and $H$.

Another, related way of determining $C$ experimentally would be the measurement of cell shape under relatively large deformations. Figure 8 shows the meridional profiles of cell shape at $\varepsilon_p = 0.2$ and 0.4 calculated for different values of $C$. At constant polar strain, the cells become progressively more conical near the poles as $C$ increases. Thus, a detailed analysis of cell profile under stress could provide a more reliable estimate of both $H$ and $B$ than simply measuring polar and equatorial strains.

## Limitations and advantages of the model

The theory, as presented, is limited to axisymmetric deformations of initially spherical cells. The restriction to initially spherical cells is not a very serious limitation, because a plasma membrane not connected to cytoplasmic elements should become spherical when it is made permeable. If this does not occur, it is evidence of an internal skeletal structure that would invalidate the basic assumption that the mechan-
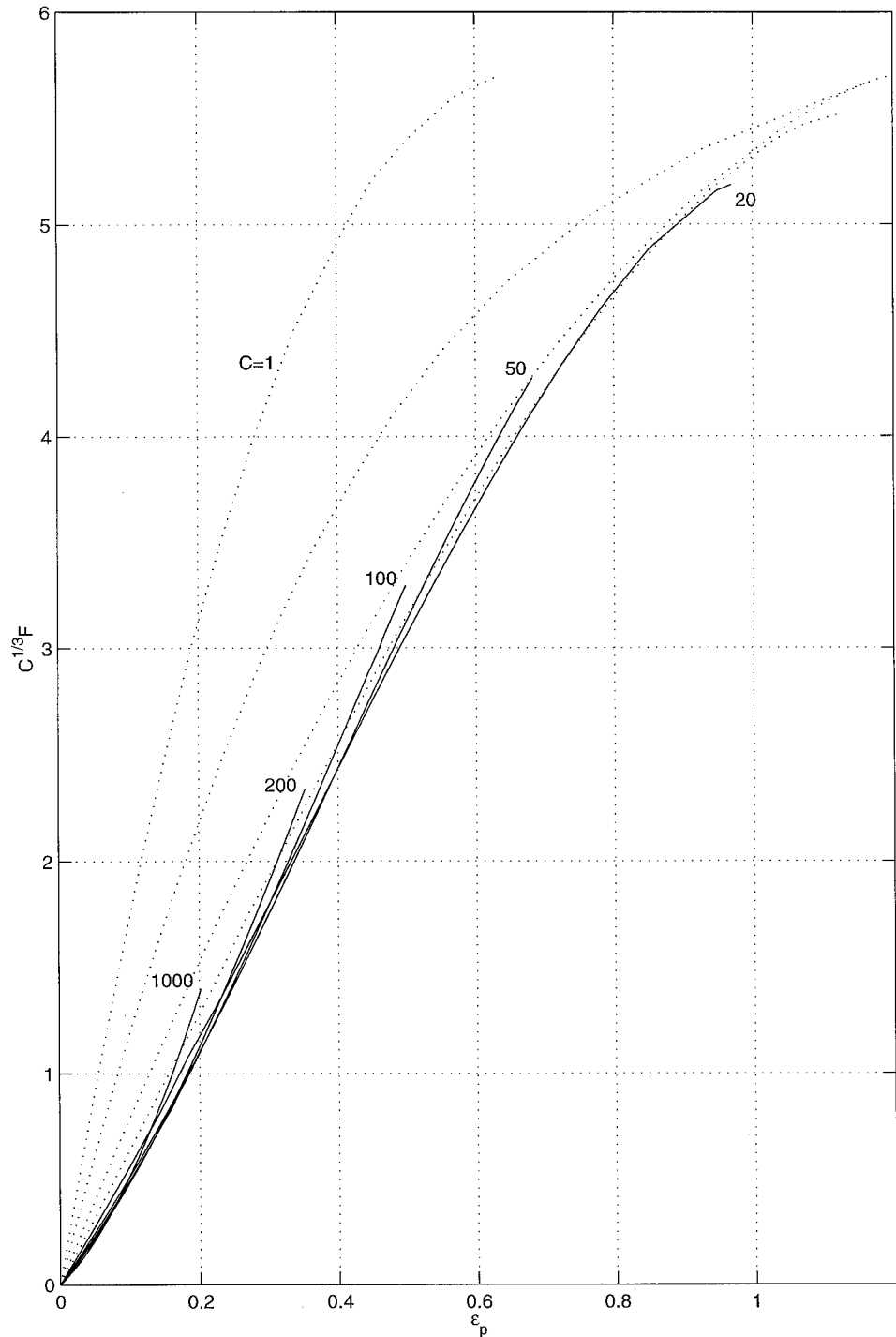
FIGURE 7  Scaled force,  $F_S = C^{1/3}F$ , plotted as a function of  $\varepsilon_p$  for  $C > 10$  (*solid lines*) showing the coalescence of the curves. The approximately linear portion of the limit curve for small  $\varepsilon_p$  is the basis of Eq. 27. The curves for  $C < 20$  are indicated by dotted lines.

ics of the cell are determined by the mechanical properties of its membrane. Although the theory is valid for arbitrarily large deformations, it is restricted to axisymmetric deformations, and this is expected to be a serious limitation when large deformations are considered. In addition, we have used the simplest, linear constitutive laws for the membrane, which would be expected to fail at the larger deformations. More realistic constitutive laws could easily be incorporated into the theory and would add only minor complications to the numerical analysis. However, without

any experimental evidence about the constitutive laws describing the behavior of the lipid bilayer membrane with its integral proteins and associated membrane skeleton, we feel that introducing more complicated material properties is currently unwarranted.

In the range over which there is a linear relationship between force and polar strain, the theory cannot determine  $H$  and  $B$  individually from the measurement of force and strain alone. However, accurate measurement of cell profile could yield this information (see Fig. 8). Alternatively, at
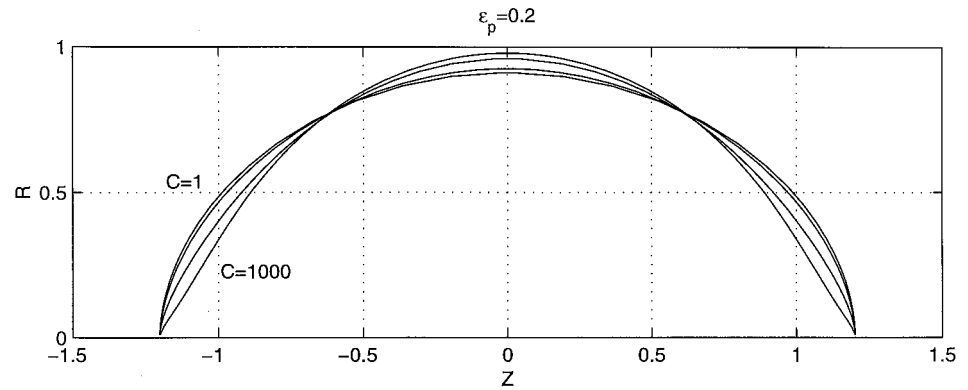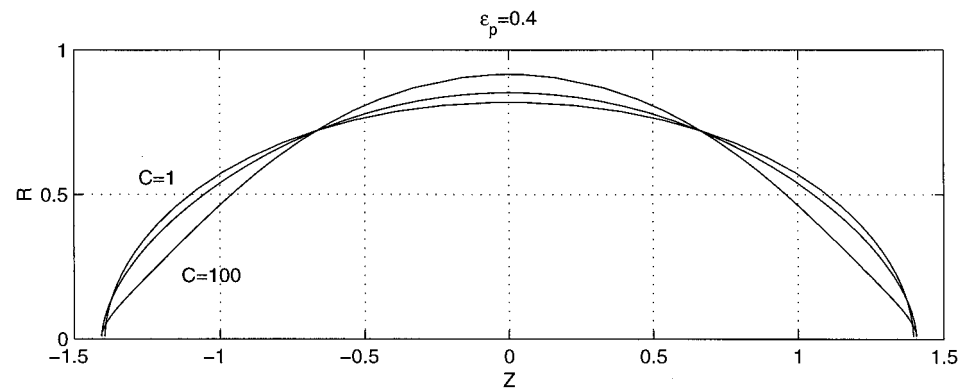
FIGURE 8 The meridional profiles of cell shapes at constant $\varepsilon_p$ for different values of $C$. (A) $\varepsilon_p = 0.2$. Profiles are shown for $C = 1$, 10, 100, and 1000. (B) $\varepsilon_p = 0.4$. Profiles are shown for $C = 1$, 10, and 100.

large strains, the nonlinear relationship between force and polar strain as a function of $C$ can differentiate the effects of $H$ and $B$. Unfortunately, experimental limitations (Sleep et al., 1999) restrict, at this stage, the scope of the applications of the theoretical treatment that we have developed. The application of higher forces, by using more intense trapping lasers, would help to separate $B$ and $H$ both by extending the force extension curve and by allowing analysis of the cell shape at higher distortions. A more precise definition of the cell profile around the point of loading would yield the required information, but explorations of this possibility must await improvements in the optical system.

Another concern in applying the model to the experiments in the accompanying paper is the nature of the attachment between the bead and membrane. We chose to model the attachment as a uniform pressure applied over a polar region of radius $\delta$. For $\delta < 0.01$, the effects were smaller than the chosen error tolerance. In some experiments, it appeared that the zone of attachment could be

considerably larger. To test whether this could have a significant effect on the predicted extensions, we carried out calculations for a series of representative conditions. For example, for $C = 100$, $F = 0.4$, we varied $\delta$ between 0.001 and 0.2 and found that $\varepsilon_P$ fell from 0.31 to 0.29. We feel that this variation is negligible in the light of the uncertainties concerning the real nature of the attachments and their effects on membrane dynamics in the attachment region that preclude more realistic modeling.

Although all of the calculations reported herein are for the case of a permeable membrane, the theory is general and valid for impermeable membranes that can develop a transmembrane pressure. Pamplona and Calladine (1996) have extended the analysis of Pamplona and Calladine (1993) to the mechanics of lobed liposomes using a cylindrical model of the deformed, impermeable liposomes. They found evidence of a buckling phenomenon, which they refer to as a "bulging tube" mode, which was on the point of buckling even under zero external pressure. It might prove possible to

extend this approach to study the stability of the equilibrium membrane configurations that we have calculated.

An interesting extension of this work could be the analysis of the transient behavior measured by Sleep et al. (1999) in response to a step-change in the applied strain. If the response of the cell was quasisteady, in the sense that it followed equilibrium deformations, it should be possible to calculate the instantaneous pressure generated within the cell by the imposed polar strain, assuming no change in cell volume. Assuming a permeability for the membrane, this pressure would induce a known flow of water through the membrane, which would reduce both the volume and the pressure within the cell resulting in a new quasisteady conformation. This process would continue until the $P = 0$ equilibrium conformation calculated herein was attained.

## REFERENCES

Boey, S. K., D. H. Boal, and D. E. Discher, 1998. Simulations of the erythrocyte cytoskeleton at large deformation. I. Microscopic models, and II. Micropipette aspiration. *Biophys. J.* 75:1573–1583 and 1584–1597.

Bozic, B., S. Svetina, and B. Zeks. 1997. Theoretical analysis of the formation of membrane microtubes on axially strained vesicles. *Phys. Rev. E.* 55:5834–5842.

Dai, J. W., and M. P. Sheetz. 1998. Cell membrane mechanics. *Method Cell Biol.* 55:157–171.

Evans, E. A., and R. Skalak. 1980. *Mechanics and Thermodynamics of Biomembranes.* Sect. 3.5. CRC Press, Boca Raton, FL.

Hansen, J. C., R. Skalak, S. Chien, and A. Hoger. 1997. Influence of network topology on the elasticity of the red blood cell membrane skeleton. *Biophys. J.* 72:2369–2381.

Iglic, A. 1997. A possible mechanism determining stability of spiculated red blood cells. *J. Biomech.* 30:35–40.

Jacoby, S. L. S., J. S. Kowalik, and J. T. Pizzo. 1972. *Iterative Methods for Nonlinear Optimization Problems.* Prentice-Hall, Englewood Cliffs, NJ, 79–83.

Pamplona, D. C., and C. R. Calladine. 1993. The mechanics of axially symmetric liposomes. *J. Biomech. Eng.* 115:149–159.

Pamplona, D. C., and C. R. Calladine. 1996. Aspects of the mechanics of lobed liposomes. *J. Biomech. Eng.* 118:482–488.

Pasternak, C., S. Wong, and E. L. Elson. 1995. Mechanical function of dystrophin in muscle cells. *J. Cell Biol.* 128:355–361.

Sleep, J., D. Wilson, R. Simmons, and W. Gratzer. 1999. Elastic properties of the red blood cell membrane and their relation to hemolytic disorders: A study by the optical tweezers technique. *Biophys. J.* 77:3085–3095.

Waugh, R. E., J. Song, S. Svetina, and B. Zeks. 1992. Local and nonlocal curvature elasticity in bilayer membranes by tether formation from lecithin vesicles. *Biophys. J.* 61:974–982.

Zeman, K., H. Engelhard, and E. Sackman. 1990. Bending undulations and elasticity of the erythrocyte membrane: effects of cell shape and membrane organization. *Eur. Biophys. J.* 18:203–219.